LETTER

Plasmonically-enhanced mid-infrared photoluminescence in a metal/narrow-gap semiconductor structure

A Letters Journal Exploring the Frontiers of Physics

May 2016

EPL, **114** (2016) 37005 www.epljournal.org
doi: 10.1209/0295-5075/114/37005

Plasmonically-enhanced mid-infrared photoluminescence in a metal/narrow-gap semiconductor structure

Pengqi Lu[1], Chunfeng Cai[1,2], Bingpo Zhang[1], Bozhi Liu[1], Huizhen Wu[1(a)], Gang Bi[2] and Jianxiao Si[3]

[1] *Department of Physics and State Key Laboratory of Silicon Materials, Zhejiang University Hangzhou, Zhejiang 310027, PRC*
[2] *Department of Information and Electronic Engineering, Zhejiang University City College Hangzhou, Zhejiang 310015, PRC*
[3] *Department of Physics, Zhejiang Normal University - Jinhua, Zhejiang 312001, PRC*

received 23 December 2015; accepted in final form 9 May 2016
published online 26 May 2016

PACS 78.55.Hx – Photoluminescence, properties and materials: Other solid inorganic materials
PACS 73.20.Mf – Collective excitations (including excitons, polarons, plasmons and other charge-density excitations)

Abstract – We report the enhancement of the mid-infrared (MIR) luminescence intensity in a nanoscale metal/semiconductor structure by the coupling of surface plasmon polaritons (SPPs) with excitons in a narrow-gap semiconductor. The SPPs are efficiently excited by the total internal reflection photons at a metal/semiconductor interface. The intense electric field induced by SPPs, in turn, greatly changes the radiative recombination rates of the excitons generated by the pumping laser and thus the MIR luminescence intensity. The finding avails the understanding of fundamental science of SPs in narrow-gap semiconductors and the development of novel MIR devices.

Surface plasmons (SPs) have recently attracted much attention due to their capabilities of confining and manipulating sub-wavelength light in the visible and infrared region [1–6]. Studies showed that when light frequencies approach the SPs resonance modes at a metal/dielectric interface, sub-wavelength confinement and internal quantum efficiency are greatly enhanced [3,7,8]. The SPs resonant coupling in metal/semiconductor structures has been extensively studied for the enhancement of luminescent efficiency of light-emitting devices (LEDs) [9–11]. However, most of these studies have focused on the visible and near-infrared region. Only a few of the studies on the enhancement of luminescent intensity in mid-infrared region are reported [6,12,13].

Lead telluride (PbTe) is a narrow-gap semiconductor and has been widely used in MIR light emitters, photonic detectors and thermoelectric devices [14–16]. However, for optoelectronic device applications, only a small fraction of emitting (or incident) photons can escape (enter) into the free space (interior of PbTe) because narrow-gap semiconductors commonly have high refractive indices ($n_{\mathrm{PbTe}} \sim 6.1$ at $3.8\,\mu$m) [17], impeding the application of optical devices based on PbTe materials. For example, to date PbTe-based LDs are almost all of low power output. In our previous work, Cai *et al.* discovered that the inherent polar CdTe/PbTe(111) interface spontaneously exhibits a metallic character with high density of electrons. A 15-fold intensity enhancement of the MIR luminescence was demonstrated by the resonant coupling between localized SPs (LSPs) at the CdTe/PbTe interface and the emitting photons from PbTe [13]. However, here a question arises, *i.e.*: can plasmons couple with MIR photons in a metal/PbTe nanostructure? In this work, we answer this key issue by the synthesis of an Ag/PbTe nanostructure and exploration of the coupling mechanism between surface plasmon polaritons (SPPs) and emitting photons from PbTe.

Six Ag/PbTe samples were fabricated for the studies of plasmonic coupling. The procedure of synthesis of the samples is as follows. First, a PbTe layer (~ 400 nm) was grown at 250 °C on a freshly cleaved BaF_2 substrate by molecular beam epitaxy, which is the same for all the samples. Then, an Ag film was deposited on the clean surface of the as-grown PbTe layers at room temperature by thermal evaporation with different Ag thicknesses for different samples, *viz.* 5, 10, 20, 50, 100 and 200 nm, respectively.

(a) E-mail: hzwu@zju.edu.cn (corresponding author)

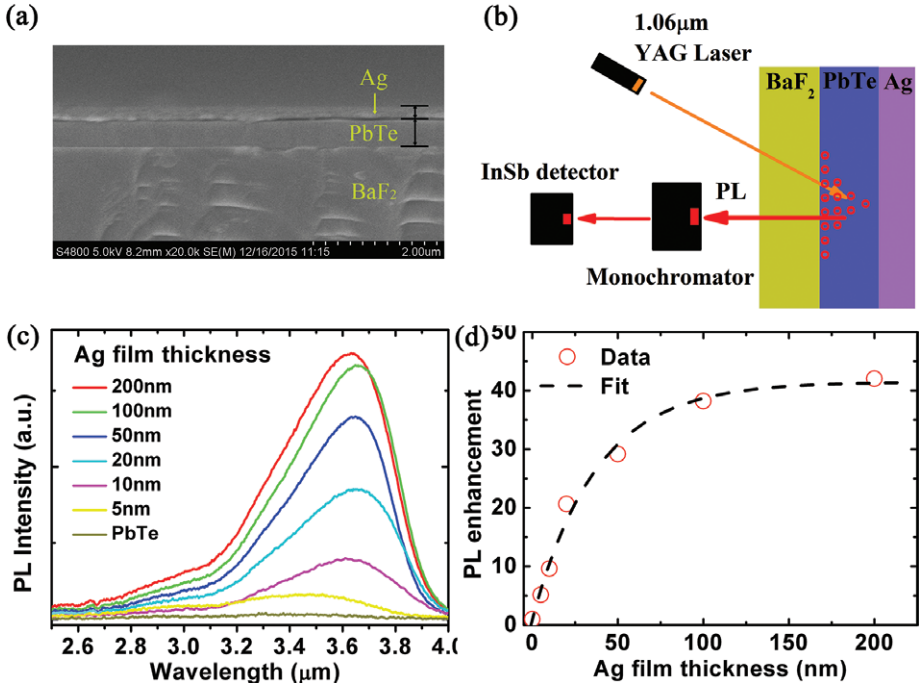

Fig. 1: (Colour online) (a) The SEM image of cross section of a Ag/PbTe sample. (b) The schematic of PL experimental setup. The red circles in the PbTe layer represent the distribution of laser excited excitons. (c) MIR PL spectra of the Ag/PbTe structures with various Ag film thicknesses. (d) Integrated MIR PL intensities *vs.* Ag film thickness.

The cross-section view of an Ag(200 nm)/PbTe(400 nm) sample by scanning electron microscope (SEM, Hitachi S4800) is shown in fig. 1(a). Photoluminescence was measured by an Edinburgh FLS920 spectrofluorimeter using the 1064 nm excitation line from a YAG laser, an InSb detector, and a Stanford SR830 lock-in amplifier. As shown in fig. 1(b), the excitation laser beam is incident from the BaF_2 substrate and the PL signal is collected from the same side.

Figure 1(c) shows the PL spectra of the six Ag/PbTe samples and a PbTe single-layer sample. Figure 1(d) plots the integrated PL intensity *vs.* the thickness of the Ag films. The fitting of the experimental data shows that the PL intensity varies in a negative exponential distribution with the increase of the Ag thickness, having the following relation: $I = -40 * \exp(-x/d_1) + 41$, where d_1 is defined as the correlation length (37 nm). When the thickness of an Ag film exceeds 200 nm, the PL enhancement factor is saturated at 40 folds. The observed intense enhancement of the MIR PL intensity could be caused by different mechanisms. First, the reflection by an Ag film on PbTe undoubtedly contributes to the MIR PL enhancement. However, the MIR reflectivity of the Ag film approximately reaches the maximum when its thickness increases to 15 nm [18], in other words the PL intensity should approach the maximum at this very thin value if the Ag reflectivity was a dominating factor in the PL enhancement, which is a far cry from the observed phenomenon: PL saturates at $\sim$ 200 nm rather than at 15 nm. Second, the BaF_2 substrate that is highly transparent for a light wavelength range of 0.3–10 μm has a much smaller refractive index than the PbTe epitaxial layer which increases the escape of the MIR light from the PbTe film to air. However, such effect should exist in all samples, including the PbTe single-layer sample, and, as a result, it cannot explain the intense enhancement of the MIR PL intensity as well. The intense enhancement of the MIR PL intensity observed in the Ag/PbTe structure is attributed mainly to the third effect, *i.e.* the coupling between SPPs and the emitting photons from PbTe. The penetration depth of SPPs in an Ag film is calculated to be 30 nm in the direction normal to the surface [19], which is close to the value derived from fig. 1(b), $d_1 = 37$ nm, suggesting that SPPs and the phenomenon of MIR PL enhancement are closely correlated.

We further performed a systematic PL characterization on the Ag(20 nm)/PbTe structure with various PbTe film thicknesses, *viz.* 120, 400, 750 and 1500 nm, respectively. It is found that the PL intensity increases slowly with the PbTe thickness at first and reaches the maximum at $\sim$ 400 nm, then it decreases sharply as shown by the (black) stars in fig. 2(a). The change of the MIR PL intensity enhancement factor *vs.* PbTe film thickness can also be explained by the SPPs coupling. With the extinction coefficient of PbTe being 1.8 at $\lambda = 1064$ nm [17], the absorption coefficient of PbTe at this excitation wavelength is calculated to be $2.216 \times 10^5\,\mathrm{cm}^{-1}$. Thus, the corresponding absorption length is 45 nm, indicating that the laser beam is mostly absorbed in the very thin PbTe region adjacent to the PbTe/BaF_2 interface and, thus,

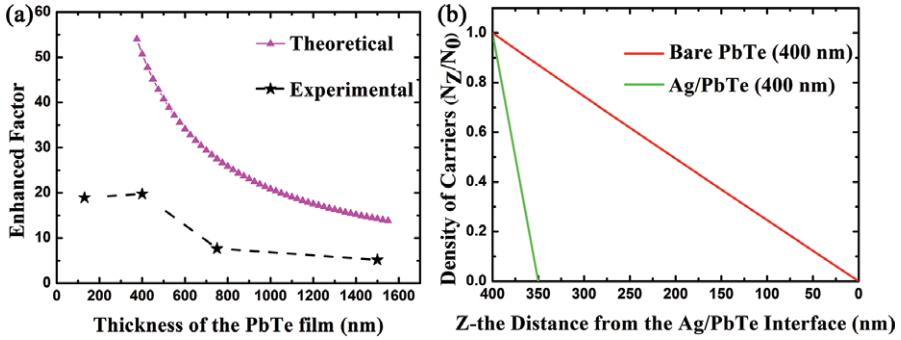

Fig. 2: (Colour online) (a) PL enhancement factor *vs.* PbTe thickness: experimental (stars) and theoretical (magenta triangles). (b) The photon-generated carriers distribution in the bare PbTe (red line) and the Ag/PbTe (green line) *vs.* the distance (Z) to the Ag/PbTe interface, which is depicted in the fig. 3(a).

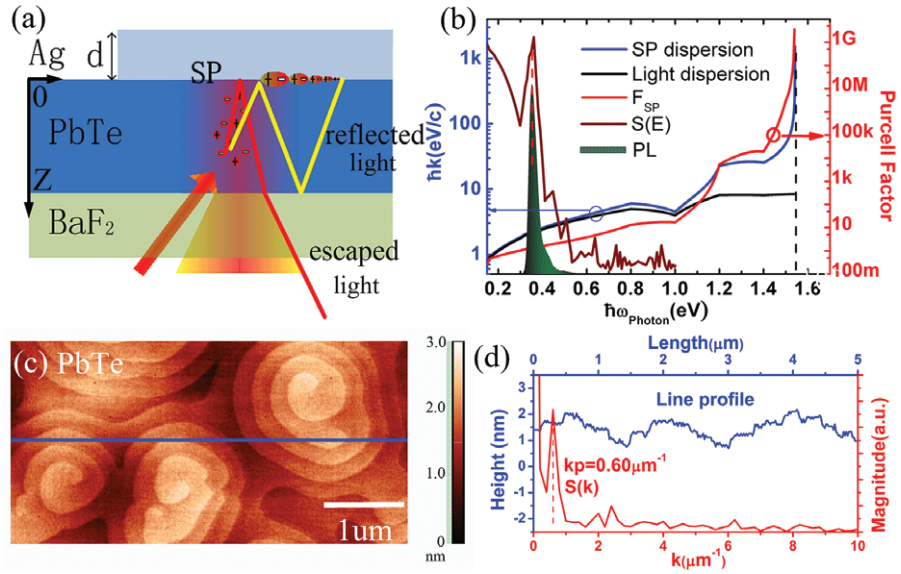

Fig. 3: (Colour online) (a) Schematic diagram of the light-SPPs coupling mechanism in the Ag/PbTe structure. The red (yellow) line stands for the escaped light (the totally reflected light). (b) SPs dispersion, structure factor $S(E)$ and Purcell factor F_{sp} at the Ag/PbTe interface, together with the dispersion of light in PbTe and the MIR PL spectrum of the Ag(200 nm)/PbTe sample. (c) An AFM image of the quasi-periodic surface of PbTe dislocations. (d) The line-scan profile of the sample along the blue line in (c) and the structure factor $S(k)$ calculated through one-dimensional discrete fast Fourier transformation of the profile shown in panel (d).

excites a large portion of excitons around the interface as shown in fig. 1(b). The excited excitons diffuse into the interior of the PbTe film and recombine gradually to be extinct. It is known that the penetration depth of SPPs in PbTe is ~ 350 nm [19], which equals the effective interacting length of SPPs in PbTe. When the PbTe thickness is beyond the SPPs interacting length, it is comprehensible that the quantity of excitons which could interact with SPPs monotonically decreases as the PbTe film becomes thicker than this value, leading to a diminution of the MIR PL intensity.

A theoretical model to estimate the PL enhancement factor is proposed by taking account of SPPs interacting with excitons and carrier diffusion in the Ag(20 nm)/PbTe(400, 750, and 1500 nm) samples. The equation of continuity for optically excited carriers in the Ag/PbTe structure can be expressed as

$$D\frac{\mathrm{d}^2N(z)}{\mathrm{d}z^2} - \frac{N(z)}{\tau} + N_0 e^{-\alpha(d-z)} = 0 \qquad (1)$$

considering the synergistic action of carrier diffusion, recombination, and light excitation, where D, z, $N(z)$, τ, α, N_0, and d are, respectively, the diffusion coefficient, the distance from the Ag/PbTe interface as shown by the Z-axis in fig. 3(a), the density of carriers *vs.* z, the lifetime of carriers, the absorption coefficient of PbTe, the density of carriers at the PbTe/BaF_2 interface, and the thickness of PbTe. The influence of the surface recombination on the carrier density is ignored here because the PbTe/BaF_2 interface grown by MBE is well

lattice-matched and smooth. The equation of $N(z)$ is then solved to be

$$N(z) = Ae^{-\left(\frac{1}{\tau D}\right)^{\frac{1}{2}}(d-z)} + Be^{\left(\frac{1}{\tau D}\right)^{\frac{1}{2}}(d-z)} - \frac{N_0}{D\alpha^2}e^{-\alpha(d-z)}, \tag{2}$$

where A and B are constants determined by specific boundary conditions. Taking the sample with PbTe thickness of 400 nm as an instance, for the bare PbTe sample the excited carriers recombine either at the Air/PbTe interface or in the PbTe film, while for the Ag/PbTe samples due to the effect of SPP coupling the carriers recombination rate within the SPP interacting region (from $Z = 0$ to 350 nm) gets intensely enhanced, so carriers can be assumed to totally recombine at $Z = 350\,\text{nm}$. Thus, the boundary conditions are $N(0) = 0; N(d = 400\,\text{nm}) = N_0$ for the bare PbTe sample and $N(d = 350\,\text{nm}) = 0; N(d = 400\,\text{nm}) = N_0$ for the Ag/PbTe (400 nm) sample. With these boundary conditions, constants A and B are knowable. The diffusion coefficient D in eq. (2) is obtained by the relation with mobility, $D = \frac{kT}{q}\mu$, where k, T, q, and μ are, respectively, the Boltzmann constant, the absolute temperature, the charge of an electron, and the mobility of carriers which was measured to be $\sim 600\,\text{cm}^2/\text{V}\cdot\text{s}$ by the Hall effect, $\tau \approx 1\,\text{ns}$. The calculated results of $N(z)/N_0$ for the bare PbTe and Ag/PbTe samples are plotted in fig. 2(b). The area beneath the red line represents the total carrier number generated in the bare PbTe, and the area beneath the green line represents the total carrier number generated in the Ag/PbTe samples. The difference of the two areas is the number of the photon-generated carriers interacting with SPPs which enhance the radiative recombination of excitons in the PbTe crystal. The power of the pumping laser for PL is about 0.1 W and the laser spot size on the samples is $\sim 2\,\text{mm}$, corresponding to an exciton generation rate of $6.25 \times 10^{17}\,\text{s}^{-1}$. The radiative recombination rate in the PbTe crystal is approximately $8.6 \times 10^{21}\,\text{cm}^{-3}\text{s}^{-1}$ [20]. The rate of excitons turning into luminescent photons is then estimated to be $1.1 \times 10^{16}\,\text{s}^{-1}$ (radiative recombination rate, $8.6 \times 10^{21}\,\text{cm}^{-3}\text{s}^{-1}$) $\times$ (volume of the region in which excitons exist, estimated by $\pi \times (1\,\text{mm})^2 \times 400\,\text{nm}$), which is only a small fraction of the excitons created in the bare PbTe (1.73%). The enhancement factors can be obtained via $\frac{P_{in}+(1-P_{in})\times 0.0173}{0.0173}$, where P_{in} is the portion of excitons interacting with SPPs. The calculation of the enhancement factors is plotted by magenta triangles in fig. 2(a) which are in qualitative agreement with the PL measurement. The difference between the calculation and the measurement results could arise from the cited old data of the radiative recombination rate for the bulk PbTe crystal [20]. The proposed theoretical model can also qualitatively explain the reported results of visible light-SP coupling experiments by Lai *et al.* [21].

Concerning the slight decrease of the PL enhancement factor of the sample with a thin PbTe layer (120 nm), two different influence factors may be involved. One is the crystalline quality deterioration of the epitaxial PbTe film if its thickness is thin, which has been systematically studied by Springholz *et al.* [22]. The other factor is that the luminescence quenching effect becomes more pronounced when radiating dipoles are too close to the metal interface [23].

A coupling mechanism of SPPs with photons in PbTe is schematically illustrated in fig. 3(a). In the single-layer PbTe sample, only a small fraction of MIR emitting light can escape into the free space, while the majority of the emitted MIR photons are repeatedly reflected within the PbTe crystal (total internal reflection, called TIR) and thermally dissipated eventually. However, in the Ag/PbTe structure things are completely different: The TIR photons possess a large momentum component in the plane parallel to the Ag/PbTe interface. Thus, the evanescent wave (or surface wave) of TIR photons at the Ag/PbTe interface has high efficiency in exciting SPPs. The electric field of the excited SPPs interacts strongly with the excitons in PbTe which are generated by the pumping laser and imposes a positive impact on the radiative recombination process [24]. Considering the penetration depth of SPPs in PbTe (350 nm), the intense electric field of SPPs interacts with excitons in almost the whole PbTe film ($\sim 400\,\text{nm}$). As a result, the MIR PL intensity in the Ag/PbTe structure is greatly enhanced. Our experimental results provide evidence supporting the theoretical prediction that SPPs are more useful to the emitters with high total internal reflection [25].

The assignment of the observed MIR PL enhancement phenomenon to the SPPs coupling effect can be supported also by the calculation of the structure factor $S(E)$. Coupling of the SPPs with MIR photons is realized by SPPs scattering from the well-regulated dislocation features on the epilayer surface as shown in fig. 3(c). These features are quasi-periodic and through one-dimensional discrete fast Fourier transformation of the line profile a structure factor $S(k)$ can be obtained as shown in fig. 3(d) [26]. Further, $S(k)$ is converted to the $S(E)$ plotted in fig. 3(b) due to the one-to-one correspondence of photon energy E and Δk, which is defined as the difference of wave vectors between light dispersion and SPs dispersion at photon energy E. A dominant peak of $S(E)$ at 0.36 eV shown in fig. 3(b) is well matched to the observed MIR PL spectrum, signifying that the quasi-periodic features can effectively scatter SPs to fulfill the conversation of momentum and thus offset the disadvantage of small Purcell factor F_{sp} (~ 1.4) for the coupling of SPPs to the MIR photons.

To analyze the influence of surface roughness on the coupling of the SPPs with MIR photons, we grew an extra PbTe sample with different surface roughness by changing substrate temperatures (280 °C). The AFM image of the sample grown at 280 °C is shown in fig. 4(a). Obviously, it has different surface morphology and roughness from fig. 3(c). The sample grown at 280 °C shows not only low-density dislocations but also high-density deep holes [27]. As shown in the inset of fig. 4(a), its structural

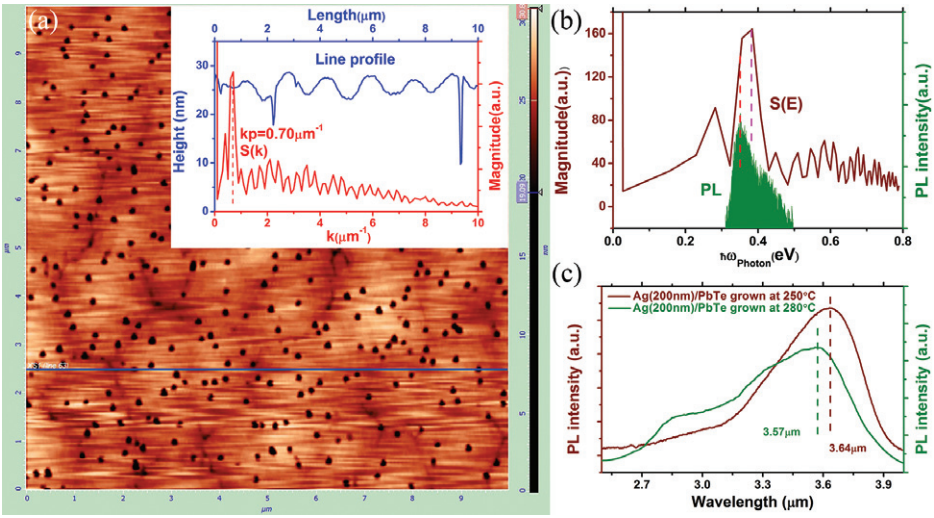

Fig. 4: (Colour online) (a) The AFM image of PbTe grown at 280 °C. The inset shows the line-scan profile along the blue line in (a) and the structure factor $S(k)$. (b) The structure factor $S(E)$ and PL of the sample shown in (a). (c) PL spectra of the two Ag(200 nm)/PbTe samples grown at 250 and 280 °C, respectively.

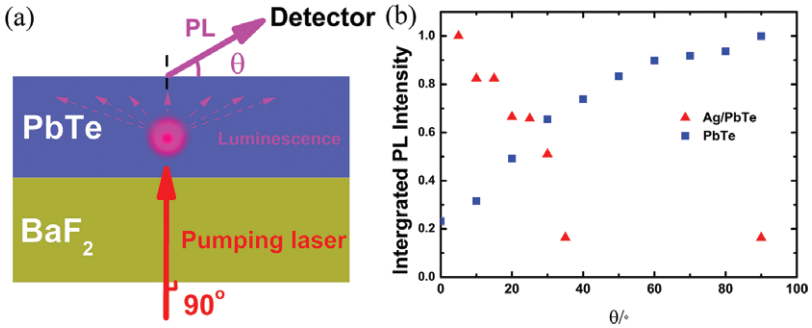

Fig. 5: (Colour online) (a) The drawing of the experimental configuration of angle-resolved PL (ARPL). (b) Integrated ARPL intensity *vs.* detection angle θ for an Ag(100 nm)/PbTe(400 nm) and a PbTe(400 nm) single layer.

factor $S(k)$ peak is at 0.7 μm^{-1}. Figure 4(b) plots the $S(E)$ peak locating at 0.38 eV, which is not far from the energy of the emitted MIR photons of PbTe, signifying that the dislocations alone can scatter SPs to fulfill the momentum conversation. Figure 4(c) shows the PL comparison of the two samples grown at different temperatures (250 and 280 °C) but the same Ag film coating (200 nm). As seen from fig. 3(c) and fig. 4(a), they present visibly different surface morphologies or different quasi-periodic surface profiles. The varied $S(E)$ for the Ag/PbTe samples causes a clear PL peak shift (70 nm) by SPP coupling: the PL peak sits at 3.64 μm (E_{ph} = 0.341 eV) for the sample grown at 250 °C and at 3.57 μm (E_{ph} = 0.347 eV) for the sample grown at 280 °C, respectively. The peak shift direction is positively correlative with the $S(E)$ peak change, 0.36 eV and 0.38 eV, respectively. The high-density holes on the surface of PbTe grown at 280 °C are deep defects which cause the decrease of the PL intensity of PbTe. The line profile density of deep holes is about 3 times that of dislocations. Thus, the $S(k)$ for holes should locate at about 2.1 μm^{-1}, corresponding to a $S(E)$ peak at 0.58 eV, which is far from the energy of the emitted MIR photons of PbTe. Consequently, these holes will disturb the scattering of SPPs related to the quasi-periodic dislocations rather than improve it. As a result, after coating an Ag film on PbTe, the measured luminescence intensity enhancement factor for this sample is small (1.8 times that of the uncoated PbTe). These results provide supporting evidence for the conclusion that the MIR photons-SPPs coupling is the dominant factor of the luminescence enhancement observed in the Ag/PbTe structure.

The MIR PL process occurred in the Ag/PbTe is further investigated by angle-resolved PL (ARPL). The schematic drawing of the ARPL configuration is shown in the inset of fig. 5(a). A pumping laser beam (λ = 1064 nm) incident from the BaF_2 substrate excites excitons in PbTe. Consequently, PbTe emits MIR photons in a 360 solid angle by the excitons recombination. The emitted MIR photons partially go forward to the Ag/PbTe interface. These MIR photons can be separated into two parts: one with incident angles smaller than the critical angle and the other with incident angles bigger than the critical angle (TIR

occurs with this part). The TIR light propagates along the interface as a surface (or evanescent) wave [28], which can efficiently excite SPPs due to frequency resonance and momentum conservation [29]. The integrated intensity of MIR ARPL *vs.* detection angle (θ) is plotted in fig. 5(b). The MIR PL intensity for the Ag/PbTe sample decreases sharply while that of the PbTe sample increases as θ becomes big. The comparison of the ARPL results for the PbTe single layer and the Ag/PbTe sample clearly shows that the coverage of an Ag film on PbTe can significantly enhance the surface wave propagating along the interface, hence the conversion to SPPs.

In summary, the intense enhancement of the MIR PL in a nanoscale Ag/PbTe structure by the interaction between SPPs and excitons in PbTe is demonstrated. The maximum enhancement factor in MIR PL is 40 folds that of the single-layer PbTe. A physical model to explain the unusual enhancement of the MIR PL in the Ag/PbTe structure is provided. The SPPs are efficiently excited by the total internal reflection photons at the Ag/PbTe interface. The intense electric field induced by SPPs, in turn, imposes a positive influence on the radiative recombination process of the excitons in PbTe and greatly enhance the MIR PL intensity. The metal/PbTe structure for SPPs-exciton coupling can also be extended to other narrow-gap semiconductors that have high refractive indices for the development of new MIR optoelectronic devices.

* * *

This work was supported by the Natural Science Foundation of China (Nos. 61290305, 11374259, and 51302248), the Foundation of Zhejiang Educational Committee (No. Y201430784).

REFERENCES

[1] Noginov M. A., Zhu G., Belgrave A. M., Bakker R., Shalaev V. M., Narimanov E. E., Stout S., Herz E., Suteewong T. and Wiesner U., *Nature*, **460** (2009) 1110.
[2] Alonso-Gonzalez P., Albella P., Schnell M., Chen J., Huth F., Garcia-Etxarri A., Casanova F., Golmar F., Arzubiaga L., Hueso L. E., Aizpurua J. and Hillenbrand R., *Nat. Commun.*, **3** (2012) 684.
[3] Okamoto K., Niki I., Shvartser A., Narukawa Y., Mukai T. and Scherer A., *Nat. Mater.*, **3** (2004) 601.
[4] Ginn J. C., Jarecki R. L., Shanner E. A. and Davids P. S., *J. Appl. Phys.*, **110** (2011) 043110.
[5] Shahzad M., Medhi G., Peale R. E., Buchwald W. R., Cleary J. W., Soref R., Boreman G. D. and Edwards O., *J. Appl. Phys.*, **110** (2011) 123105.
[6] Stanley R., *Nat. Photon.*, **6** (2012) 409.
[7] Okamoto K., Niki I., Scherer A., Narukawa Y., Mukai T. and Kawakami Y., *Appl. Phys. Lett.*, **87** (2005) 071102.
[8] Okamoto K., *Surface Plasmon Enhanced Solid-State Light-Emitting Devices*, in *Nanoscale Photonics and Optoelectronics: Science and Technology*, edited by Wang Z. M. and Neogi A. (Springer, New York) 2010.
[9] Barnes William L., Dereux Alain and Ebbesen Thomas W., *Nature*, **424** (2003) 824.
[10] Gontijo I., Boroditsky M. and Yablonovitch E., *Phys. Rev. B*, **60** (1999) 11564.
[11] Kwon Min-Ki, Kim Ja-Yeon, Kim Baek-Hyun, Park Il-Kyu, Cho Chu-Young, Byeon Clare Chisu and Park Seong-Ju, *Adv. Mater*, **20** (2008) 1253.
[12] Das N. C., *Infrared Phys. Technol.*, **55** (2012) 166.
[13] Cai C. F., Jin S. Q., Wu H. Z., Zhang B. P., Hu L. and McCann P. J., *Appl. Phys. Lett.*, **100** (2012) 182104.
[14] Tamura W., Itoh O., Nugraha, Suto K. and Nishizawa J., *J. Electron. Mater*, **28** (1999) 907.
[15] Yasuda A., Suto K. and Nishizawa J., *J. Mater. Sci. Semicond. Process.*, **27** (2014) 159.
[16] Khiar A., Eibelhuber M., Volobuev V., Witzan M., Hochreiner A., Groisss H. and Springholz G., *Opt. Lett.*, **39** (2014) 6577.
[17] Palik E. D., *Handbook of Optical Constants of Solids* (Academic Press, San Diego) 1998.
[18] Zhao Q. N., Ma M. M., Dong Y. H., Wang Z. D., Zhao X. J. and Gao B. X., *J. Wuhan Univ. Technol.*, **31** (2009) 75.
[19] Raether H., *Springer Tracts Mod. Phys.*, Vol. **111** (Springer) 1988, p. 1.
[20] Mackintosh I. M., *Proc. Phys. Soc. B*, **69** (1956) 115.
[21] Lai C. W., An J. and Ong H. C., *Appl. Phys. Lett.*, **86** (2005) 251105.
[22] Springholz G., Ueta A. Y., Frank N. and Bauer G., *Appl. Phys. Lett.*, **69** (1996) 2822.
[23] Sun G., Khurgin J. B. and Yang C. C., *Appl. Phys. Lett.*, **95** (2009) 171103.
[24] Kim D., Yokota H., Taniguchi T. and Nakayama M., *J. Appl. Phys*, **114** (2013) 154307.
[25] Khurgin Jacob B., Sun Greg and Soref Richard A., *J. Opt. Soc. Am. B*, **24** (2007) 1968.
[26] Shubina T. V., Gippius N. A., Shalygin V. A., Andrianov A. V. and Ivanov S. V., *Phys. Rev. B*, **83** (2011) 165312.
[27] Xu T. N., Wu H. Z., Si J. X. and Cao C. F., *Appl. Surf. Sci.*, **253** (2007) 5457.
[28] Hecht Eugene, in *Optics*, 4th edition (Addison-Wesley, San Francisco) 2002, p. 125.
[29] Otto A., *Z. Phys.*, **216** (1968) 398.